Triangular Springs for Modeling Non-Linear Membranes

H. Delingette

Asclepios Research Project, INRIA, 06902 Sophia Antipolis, France

***Abstract*— This paper provides a formal connexion between springs and continuum mechanics in the context of one-dimensional and two-dimensional elasticity. In a first stage, the equivalence between tensile springs and the finite element discretization of stretching energy on planar curves is established. Furthermore, when considering a quadratic strain function of stretch, we introduce a new type of springs called tensile *biquadratic springs*. In a second stage, we extend this equivalence to non-linear membranes (St Venant-Kirchhoff materials) on triangular meshes leading to triangular biquadratic and quadratic springs. Those tensile and angular springs produce isotropic deformations parameterized by Young modulus and Poisson ratios on unstructured meshes in an efficient and simple way. For a specific choice of the Poisson ratio, 0.3, we show that regular spring-mass models may be used realistically to simulate a membrane behavior. Finally, the different spring formulations are tested in pure traction and cloth simulation experiments.**

***Index Terms*— spring-mass, membrane, St-Venant Kirchhoff, biquadratic springs, TRBS, TRQS, cloth simulation.**

I. Introduction

In recent years, computer graphics has tackled the tough challenge of simulating the deformation of flexible objects, sometimes in real-time, by developing a wide variety of physically based models [1]. In fact, some of those models are not strictly based on the law of physics but a growing number are borrowed or inspired from mechanical engineering and especially from continuum mechanics. If we only focus on simulating the deformation of surface objects, the mechanical theory of interest is the theory of plates and shells [2]. Plates and shells are volumetric bodies whose thickness is small compared to their extent, plates being flat surfaces that can bend or twist and shells being curved smooth surfaces. Because the computer graphics community is mainly interested in simulating the deformation of clothes or anatomical membranes the focus has mainly been on the shell theory. In this framework, the energy necessary to deform a shell can be decomposed into the sum of a membrane energy and a bending energy. The membrane term corresponds to the in-plane stretching energy and requires only first order derivatives of the displacement. On the other hand, the bending energy is related with the variation of surface curvature and involves second-order derivatives. There exists several thin shell models associated with different kinematic hypothesis. One common choice is the Kirchhoff-Love thin shell theory [3] where lines initially normal to the middle surface are assumed to remain straight after deformation, to keep their initial length and to remain normal to the middle surface. For instance, Eischen [4] has modelled cloth deformation based on the Kirchhoff-Love thin shell theory . Cirak [5] *et al.* have used subdivision surfaces to discretize the developed Kirchhoff-Love energy without including any nodal rotations. This work was extended by Green [3] to include quadrilateral elements and better enforcements of boundary conditions.

Despite the development of those rather complex "physically-based" models, a large number of animation systems are still largely based on the mass-springs, because they are supposedly both simple to understand and to implement. Mass-springs models are essentially discrete models that define elastic forces between two vertices based on the variation of the edge length. Although spring forces are related to the theory of one-dimensional elasticity (see section II), they cannot be used to discretize properly two or three dimensional elastic materials based on continuum mechanics. Van Gelder [6] showed for instance that spring-mass models cannot represent linear elastic membranes but proposed a spring stiffness formulation that approximate the membrane behavior (see section IV-B). The discrete nature of spring-mass systems is particularly problematic when handling unstructured triangular or tetrahedral meshes. To cope with this limitation, a number of researchers [7], [8] have proposed computational methods to estimate the topologies and the stiffness of springs. But a more common alternative is to define springs on a rectangular [9], [10] or hexahedral lattice [11] in order to improve the isotropy and homogeneity of the deformation.

Knowing the limitations of mass-springs models, several authors have developed "particle systems" [1], closely related to the intuitive notion of springs but that are more physically plausible without resorting to the complexity of the Kirchhoff-Love models. Terzopoulos *et al.* [9] in 1988, for instance, proposed a membrane (resp. bending) energy which corresponds to the weighted norm of the difference between the first (resp. second) fundamental form of the deformed configuration and that of the rest configuration. Those deformation energies were discretized and approximated with finite differences on a regular grid. Provot [12] and Breen [13] proposed to include some non-linear effects in the stiffness of mass springs models in order to better simulate cloth deformation. Baraff and Witkin [14] replaced the membrane energy introduced in [9] which is a quartic function of position with a quadratic function but which is only valid for small deformation. Eischen [15] compared finite elements and modified mass spring models on a regular lattice and showed similar behavior. Bourguignon *et al.* [16] have proposed to include anisotropic behavior in mass springs models by adding angular springs.

Volino [17] used a linear strain-stress relationship to model cloth deformation and later [18] proposed a membrane energy on non-regular triangular meshes that couples the elongation of all triangle edges. Etzmuss [19] *et al.* have carefully derived a particle system from the equations of continuum mechanics on a regular surface grid. They approximate the strain tensor by defining a sheared rest frame and derive a formulation where tension and shearing forces are computed from the dot product of edge vectors. Grinspun [20] *et al.* have defined a membrane energy that penalizes the change of edge elongation and triangle area, similarly to the approach proposed by Teschner [21], and a bending energy related with the change of dihedral angle of each triangle edge. Etzmuss *et al.* [22] use a corotational approach to apply the linear elastic membrane formulation even in case of large rotation of triangles. Thomaszewski [23] *et al.* extended the corotational principle to the linearized Kirchhoff-Love model discretized with subdivision surfaces. Bridson [24] *et al.* have introduced bending forces that minimize the variation of the dihedral angle around each edge, while Choi [25] use non-linear springs for the membrane and bending energies on a regular lattice to cope with the post-buckling instabilities of fabrics. Volino [26] proposed linearized bending forces that are suited for implicit time integration.

The models mentioned above are inspired from continuum mechanics and have some nice properties in the context of Computer Graphics : they are usually invariant with respect to rigid transformations and they are often simple to implement, relatively efficient to compute and lead to plausible deformations. However, those models do not follow the laws of continuum mechanics or only on restricted cases (small displacements,...). As such, they lack one essential property : the deformation of a model based on continuum mechanics only depends on its number of degrees of freedom but not on the discretization method. This is a very important property since it allows to build efficient algorithms based on multigrid approaches [27], adaptive refinement methods [28] or to combine two different discretization methods in the same object (*e.g.* hybrid models in [29]). Furthermore continuum models guarantee the true isotropy or anisotropy of the material which is often difficult to enforce with discrete models. .

Dealing with continuum models instead of discrete ones has been reported in many computer graphics papers as being far more complex and as leading to greater computation times. While this is true in general, for specific choices of the discretization method (constant strain finite element method), continuum models may actually be as simple and even more efficient [29] than mass spring models (see section V-A).

In this paper, we show the *total equivalence* between a continuum formulation of the membrane energy and the energy of a set of *triangular biquadratic springs*. Those springs do not correspond exactly to the regular springs that are commonly encountered in computer graphics. However, we show that for small deformations, they are equivalent to regular (quadratic) tensile and angular springs. Furthermore, triangular biquadratic springs are simple to implement and efficient to compute and they have a similar complexity than that mass spring models, even if they are continuum models based on non-linear, finite strain mechanics.

To derive these new spring models, we first look at the theory of one-dimensional elasticity and show how it is closely related to the concept of springs. In section III, a non-linear membrane energy on two-dimensional manifolds is described and a formal equivalence of that strain energy and biquadratic springs is established when discretized with the finite element method on linear triangles. In section IV, two limit cases of that strain energy are studied : small displacements and small deformations. In the latter case, equivalence with regular tensile and angular springs is established. Finally, in section V, we benchmark the different membrane formulation in test cases but also in the context of cloth simulation.

II. Springs and One-Dimensional Elasticity

A. Linear Elastic Axially Loaded Bar

In this section, we detail how a linear elastic material under large displacements is formulated for an axially loaded bar which is clamped on one side. The bar is assumed to have constant cross-sectional area A, the center of each cross-sections being on a straight line (see Figure 1) of length L. The rest configuration of the bar is $\Omega \subset \mathbb{R}^3$ and after applying an axial load, each center of cross-sections $\mathbf{X} \in [0, L]$ is moved into a new position $\mathbf{\Phi}(\mathbf{X}) \in [0, \mathbf{\Phi}(L)]$. An infinitesimal material segment of length dx and located around center point $\mathbf{X}$ is deformed into a segment of length $\frac{d\mathbf{\Phi}}{dx}(X)\ dx$. The stretch ratio s is thus $s = \frac{d\mathbf{\Phi}}{dx}$. When this stretch ratio is exactly one then the deformation does not entail any local stretching effect around point $\mathbf{X}$. The strain ϵ at this point is a quantity that measures how different is this stretch ratio from the value one, positive strain implying extension of the material and negative strain contraction. There exists a family of possible strain functions :

$$\epsilon(C) = \left\{ \begin{array}{ll} \frac{1}{\alpha}\left(s^\alpha - 1\right) & \text{if } \alpha \neq 0 \\ \log(s) & \text{if } \alpha = 0 \end{array} \right\}$$

When $\alpha = 1$, $\epsilon = s - 1$, it is called the engineering strain. For $\alpha = 2$ $\epsilon = 1/2(s^2 - 1)$, it corresponds to the Green-Lagrange strain while $\alpha = 0$ corresponds to the Henky or natural strain. The engineering strain is maybe the most intuitive strain measure since it corresponds to a relative length variation however it does not generalize easily to 2D or 3D elastic materials. The Green-Lagrange strain on the other hand is the most widely used because it is analytically tractable but it leads to non-intuitive behavior for strong compression. Henky strain leads to more complex computations but possesses many remarkable properties [30].

Making the hypothesis of a linear elastic material, the (nominal) stress (force per unit area) $\sigma(\mathbf{X})$ at each point is proportional to the strain at that point : $\sigma = \lambda\epsilon$ where λ is a stiffness parameter (in Nm^{-2}). The work W necessary to bring the material cross section around center point $\mathbf{X}$ to $\mathbf{\Phi}(\mathbf{X})$ is therefore $W = \frac{1}{2}\sigma\epsilon$ and the total energy W_Ω required to deform the bar Ω, assumed to be homogeneous, is :

$$W_\Omega = \int_\Omega \frac{1}{2}\sigma\epsilon\ dV = \frac{\lambda A}{2\alpha^2}\int_0^L \left((\frac{d\mathbf{\Phi}}{dx})^\alpha - 1 \right)^2 d\mathbf{X}$$

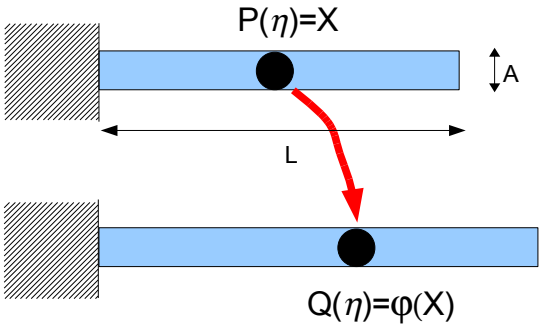

Fig. 1. Axially loaded bar in rest (top) and deformed (bottom) configurations. All cross sections are identical and of area A. The center line is a segment of rest length L and is parameterized with function $P(\eta)$ (resp. $Q(\eta)$), $\eta \in [a,b]$ in its rest (resp. deformed) position.

If the segment $[0,L]$ is parameterized by a function $\mathbf{X} = P(\eta), \eta \in [a,b] \subset \mathbb{R}$ and its deformation by a function $\mathbf{\Phi}(\mathbf{X}) = Q(\eta), \eta \in [a,b] \subset \mathbb{R}$ then the deformation function can be written as : $\mathbf{\Phi}(\mathbf{X}) = Q(P^{-1}(\mathbf{X}))$. In this case, the total energy W_Ω can be expressed as :

$$W_\Omega = \frac{\lambda A}{2\alpha^2} \int_a^b \left((\frac{dQ}{d\eta})^\alpha - (\frac{dP}{d\eta})^\alpha \right)^2 \left(\frac{dP}{d\eta} \right)^{(1-2\alpha)} d\eta \quad (1)$$

B. Stretching energy of deformable curves

Instead of studying the deformation of a straight bar, we consider a curved bar Ω of cross-section A embedded in a Euclidean space $\mathbb{R}^d$, $d > 1$. The center line curve parameterized as $\mathbf{P}(\eta)$, is deformed into another curve $\mathbf{\Phi}(\Omega)$, parameterized with $\mathbf{Q}(\eta)$, $\eta \in [a,b]$. To obtain the stretching energy necessary to deform Ω into $\mathbf{\Phi}(\Omega)$, it suffices to replace in Equation 1 the first derivative $\frac{dP}{d\eta}$ with the norm of the first derivative $\|\frac{d\mathbf{P}}{d\eta}\|$:

$$W_\Omega = \frac{\lambda A}{2\alpha^2} \int_a^b \left(\|\frac{d\mathbf{Q}}{d\eta}\|^\alpha - \|\frac{d\mathbf{P}}{d\eta}\|^\alpha \right)^2 \left\| \frac{d\mathbf{P}}{d\eta} \right\|^{(1-2\alpha)} d\eta \quad (2)$$

If the parameter η is the arc length of the reference curve $\mathbf{P}(\eta)$ then the stretching energy simplifies as :

$$W_\Omega = \frac{\lambda A}{2\alpha^2} \int_\Omega \left(\|\frac{d\mathbf{Q}}{d\eta}\|^\alpha - 1 \right)^2 d\eta \quad (3)$$

Clearly, this functional is zero if the arc length of $\mathbf{P}(\eta)$ is also the arc length of deformed curve $\mathbf{Q}(\eta)$

C. Finite Element Discretization

We use in the remainder the Rayleigh-Ritz approach [31](p 60) of the finite element method. This approach is equivalent to the Galerkin weighted residual method, and relies on the variational form (strain energy) rather than the weak form (principle of virtual work) of the same elasticity problem. Dealing with the variational form is more convenient to derive symmetric analytical expressions and is widely used in computer graphics. Equations are derived by first discretizing the stretching energy and then applying the principle of minimum potential energy.

In Equation 2, the coordinate functions $\mathbf{P}(\eta)$ and $\mathbf{Q}(\eta)$ only need to have their first derivative square integrable. Therefore, the reference curve Ω can be approximated with a set Ω_h of line segments S_i : $\Omega^h = \bigcup_{i=1,..,N} S_i = [\mathbf{P}_i, \mathbf{P}_{i+1}]$. Each reference segment $[\mathbf{P}_i, \mathbf{P}_{i+1}]$ is deformed into segment $[\mathbf{Q}_i, \mathbf{Q}_{i+1}]$, the set of points $\{\mathbf{Q}_i\}$, $i = 1, \ldots, N$ being the nodes of the finite element model.

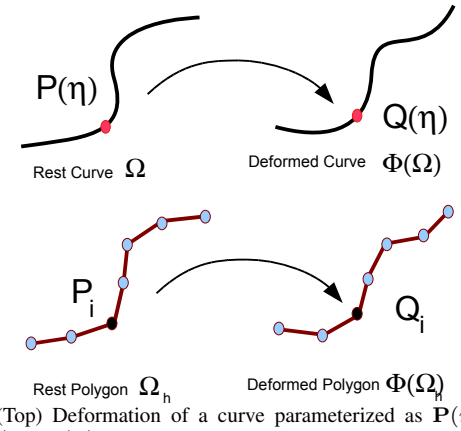

Fig. 2. (Top) Deformation of a curve parameterized as $\mathbf{P}(\eta) \in \Omega$ into curve $\mathbf{Q}(\eta) \in \mathbf{\Phi}(\Omega)$; (Bottom) Discretization of the domain Ω as a set of line segments Ω_h. The deformed positions $\{\mathbf{Q}_i\}$ are the nodes (unknown variables) of the finite element model.

Each segment in the reference or deformed configuration can be parameterized as a linear interpolation :

$$\mathbf{P}(\eta) = (1-\eta)\mathbf{P}_i + \eta\mathbf{P}_{i+1}$$
$$\mathbf{Q}(\eta) = (1-\eta)\mathbf{Q}_i + \eta\mathbf{Q}_{i+1}$$

To simplify notations, we write $L_i = \|\mathbf{P}_i\mathbf{P}_{i+1}\|$ the length of the rest segment and $l_i = \|\mathbf{Q}_i\mathbf{Q}_{i+1}\|$ the length of the deformed segment.

The stretching energy W_{Ω_h} of the discretized domain Ω_h is the sum of the stretching energy of each line segment $W_{\Omega_h}(S_i)$. Because the first derivative is constant on each element, the stretch ratio of each point in segment S_i is simply l_i/L_i and therefore the stretching energy $W_{\Omega_h}(S_i)$ is :

$$W_{\Omega_h}(S_i) = \frac{\lambda A L_i^{(1-2\alpha)}}{2\alpha^2} \left(l_i^\alpha - L_i^\alpha\right)^2 \quad (4)$$

For engineering strain ($\alpha = 1$), the stretching energy therefore corresponds to the energy of a spring of stiffness $\lambda A/L_i$. Thus a set of masses along a curve that are connected with springs corresponds to the discretization of the stretching energy of that curve for engineering strain. When the first variation of the energy given in equation 3 is considered, we find the same expression as the one dimensional wave equation found by Etzmuss *et al.* [19] :

$$\delta W_{\Omega_h}(S_i) = \lambda A (\frac{d^2\mathbf{Q}}{d\eta^2} - \frac{d\mathbf{t}_Q}{d\eta})$$

where $\mathbf{t}_Q$ is the tangent vector at point $\mathbf{Q}(\eta)$.

For Green-Lagrange strain ($\alpha = 2$) however, the stretching energy is a biquadratic function of the deformed segment length l_i and of the deformed position $\mathbf{Q}_i$:

$$W_{\Omega_h}(S_i) = \frac{\lambda A}{8L_i^3} \left(l_i^2 - L_i^2\right)^2 \quad (5)$$

Because this expression resembles to a (quadratic) spring energy but with squared lengths, it is coined as a tensile *biquadratic spring*. To study the difference between regular (or quadratic) and biquadratic springs, it is convenient to write each stretching energy as a function of the stretch ratio s. In both cases, the stretching energy can be written as :

$$W_{\Omega_h}(S_i) = \lambda A L_i \; w(s)$$

where $w(s) = w_Q(s) = 1/2(1-s)^2$ for quadratic springs and $w(s) = w_B(s) = 1/8(1-s^2)^2$ for biquadratic springs. From the graphs of Figure 3, one can see that for large extension of those springs, $s > 1.2$, both energies increase sharply, biquadratic springs being far more stiffer than quadratic springs. For large compression, where the stretch ratio is below 0.8, they behave quite differently : the quadratic springs lead to a force proportional to the stretch ratio while for the biquadratic springs, the compression force reaches a maximum for $s = \sqrt{2}/2$ and then decreases toward zero as the stretch ratio decreases toward zero (see Figure 3 (right)). Therefore, biquadratic springs have a rather unphysical behavior when compressed since an increase of compression creates a decrease of the elastic force when $s < \sqrt{2}/2$ (see [**?**] for similar comments). Quadratic springs can also be qualified as unphysical since a finite amount of energy is sufficient to produce a full compression of the material, *i.e.* $s = 0$. Only the logarithm strain function leads to a plausible elastic energy: this is why it has been qualified as *natural strain*.

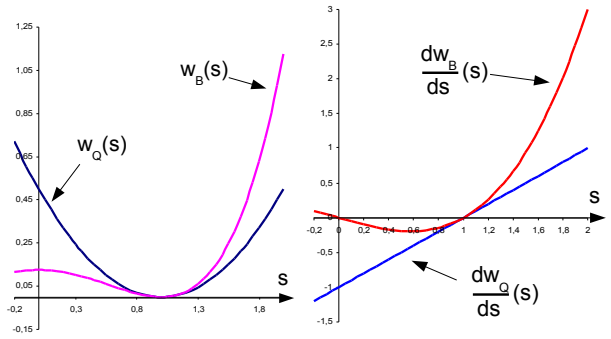

Fig. 3. (Left) Graphs of the energy functions for quadratic springs $w_Q(s)$ and biquadratic springs $w_B(s)$;(Right) Graphs of their derivatives

If we make the hypothesis that each segment undergoes small deformations but possibly large displacements, $s \approx 1$, then we can make the following approximation : $l_i^2 - L_i^2 \approx 2L_i\,(l_i - L_i)$. In this case, the energies of the quadratic and biquadratic springs are becoming equivalent. In fact, given that all strain functions have the same first and second derivatives around $s = 1$, the stretching energy for small deformations is independent on the choice of the strain function.

D. Linear Elasticity : small displacements hypothesis

We now make an even more restrictive hypothesis regarding the deformation of the curve : we assume that all vertex displacement $\mathbf{U}_i = \mathbf{Q}_i - \mathbf{P}_i$ is small compared to the edge length L_i. Replacing each vertex position $\mathbf{Q}_i$ by $\mathbf{P}_i + \mathbf{U}_i$, we make the following approximation :

$$l_i^\alpha \approx L_i^\alpha + \alpha L_i^{(\alpha-2)} (\mathbf{U}_{i+1} - \mathbf{U}_i) \cdot (\mathbf{P}_{i+1} - \mathbf{P}_i)$$

Therefore for small displacements, all strain functions can be approximated as the same linear function of displacement :

$$(s^\alpha - 1)/\alpha \approx (\mathbf{U}_{i+1} - \mathbf{U}_i) \cdot (\mathbf{P}_{i+1} - \mathbf{P}_i)/L_i^2$$

In such case, the strain is a linear function of displacement but also of stress : this is why such model is called a linear elastic model. Its stretching energy is a quadratic function of displacements :

$$W_{\Omega_h}^{\text{Linear}}(S_i) = \frac{\lambda A}{L_i^3} \left((\mathbf{U}_{i+1} - \mathbf{U}_i) \cdot (\mathbf{P}_{i+1} - \mathbf{P}_i) \right)^2$$

To summarize, one dimensional elasticity on curves (stretching term) can be discretized with springs given the following choices :

- Linear relation between strain and stress
- Linear element for the finite element discretization
- Large displacement hypothesis (finite strain)

For Green-Lagrange strain, the finite-element method leads to the biquadratic springs while for engineering strain, it leads to regular (or quadratic) springs. Finally, there exists two limit cases that are independent on the choice of the strain function : the hypothesis of small deformations and of small displacements.

III. Membrane Energy on Triangular Meshes

A. Membrane Energy

The energy necessary to deform a piece of cloth or paper can be decomposed into different components : a membrane energy which characterizes the resistance to in-plane stretching and a bending energy which measures the resistance to change in the surface normal orientation. The membrane energy generalizes the stretching energy for curves and under the plane stress hypothesis [31] (p87), this energy only depends on the change in local metrics of the surface (its first fundamental form).

We consider a two-dimensional compact domain $\Omega \subset \mathbb{R}^2$ being deformed into another domain $\mathbf{\Phi}(\Omega)$. A material point $\mathbf{X} \in \Omega$ is moved to a new position $\mathbf{\Phi}(\mathbf{X}) \in \mathbf{\Phi}(\Omega)$, the function $\mathbf{\Phi}(\mathbf{X})$ being the deformation function. Similarly to the stretch ratio s for the one-dimensional case, the relative change of length around point $\mathbf{X}$ is captured by the spatial derivative of the deformation function. However, because the domain Ω is two-dimensional, this quantity is now a two dimensional tensor, the *right Cauchy-Green deformation tensor* $\mathbf{C}$, defined as : $\mathbf{C} = \nabla\mathbf{\Phi}^T \nabla\mathbf{\Phi}$

This tensor is equivalent to the square stretch ratio s for one dimensional elasticity and it naturally leads to the *Green-Lagrange strain tensor* $\mathbf{E}$: $\mathbf{E} = 1/2(\mathbf{C} - \mathbf{I})$. Despite the existence of other strain tensors [32], they often do not lead to closed-form expressions. The Green-Lagrange strain tensor is invariant to the application of translations or rotations and is therefore appropriate for describing deformations under large displacements.

Assuming an isotropic St Venant Kirchhoff membrane for which there is a linear relationship between the amount of

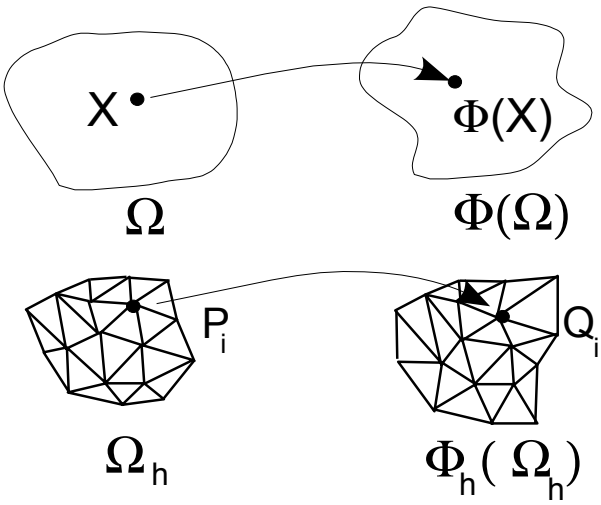

Fig. 4. (Top) Definition of the deformation function $\mathbf{\Phi}(\mathbf{X})$ that maps the rest domain Ω into the deformed domain $\mathbf{\Phi}(\Omega)$. (Bottom) Same definition after discretizing the domain Ω into a conformal triangulation Ω_h.

stress and the amount of strain, the density of membrane energy $W(\mathbf{X})$ can be written as :

$$W(\mathbf{X}) = \frac{\lambda}{2}(tr\mathbf{E})^2 + \frac{\mu}{2}tr\mathbf{E}^2 \tag{6}$$

where λ and μ are the Lamé coefficients of the material. Those coefficients are simply related to the physically meaningful Young modulus E and Poisson coefficient ν : $\lambda = \frac{E\nu}{1-\nu^2}$ and $\mu = \frac{E(1-\nu)}{1-\nu^2}$. The Young modulus quantifies the stiffness of the material while the Poisson coefficient characterizes the material compressibility ($\nu = 1.0$ for an incompressible material).

The total membrane energy W_Ω consists in summing the density of energy over the whole domain :

$$W_\Omega = \int_\Omega W(\mathbf{X})\ d\Omega = \int_\Omega \left(\frac{\lambda}{2}(tr\mathbf{E})^2 + \frac{\mu}{2}tr\mathbf{E}^2\right)\ d\Omega$$

B. Deformation function on a Linear Triangle

Since the density of membrane energy involves the integration of first derivatives of the deformation function $\mathbf{\Phi}$, the domain Ω is discretized into a simplicial surface Ω_h consisting of a set of triangles $\{T_i\}, i = \{1, .., p\}$ and a set of vertices $\{\mathbf{P}_i\}, i \in \{1, .., n\}$.

We choose the linear triangle element for discretizing the surface since it is the simplest two-dimensional continuum element and leads to closed form stiffness matrices. Thus, a functional space S_h of finite dimension is defined as a set of functions that are C^0 on Ω_h and that are linear of each triangle. A deformation function $\mathbf{\Phi}_h \in S_h$ is uniquely determined by its nodal vector $\{\mathbf{Q}_i\}, i \in \{1, .., n\}$ such that $\mathbf{Q}_i = \mathbf{\Phi}_h(\mathbf{P}_i)$.

To compute the total membrane energy $W(\Omega_h)$ we must evaluate the membrane energy necessary to deform a single triangle T_P consisting of vertices $\{\mathbf{P}_1, \mathbf{P}_2, \mathbf{P}_3\}$ into its deformed position T_Q with vertices $\{\mathbf{Q}_1, \mathbf{Q}_2, \mathbf{Q}_3\}$ (see Figure 5). We write as $\mathcal{A}_P$ (resp. $\mathcal{A}_Q$) the area of the rest triangle T_P (resp. triangle T_Q), l_i (resp. L_i) its edge length and α_i (resp. β_i) its 3 angles.

Any point $\mathbf{X} = (x, y)^T$ in the rest triangle T_P can be parameterized with its barycentric coordinates $\eta_i(\mathbf{X})$ such that :

$$\begin{bmatrix} x \\ y \\ 1 \end{bmatrix} = \begin{bmatrix} \mathbf{P}_{1x} & \mathbf{P}_{2x} & \mathbf{P}_{3x} \\ \mathbf{P}_{1y} & \mathbf{P}_{2y} & \mathbf{P}_{3y} \\ 1 & 1 & 1 \end{bmatrix} \begin{bmatrix} \eta_1 \\ \eta_2 \\ \eta_3 \end{bmatrix} = [\overline{\mathbf{P}}]\ \ \overline{\mathbf{E}} \tag{7}$$

The inverse relation defines the barycentric coordinates of any point $\mathbf{X} \in T_P$ given that the triangle is not degenerate :

$$\begin{bmatrix} \eta_1 \\ \eta_2 \\ \eta_3 \end{bmatrix} = \begin{bmatrix} \mathbf{D}_{1x} & \mathbf{D}_{1y} & \eta_1^0 \\ \mathbf{D}_{2x} & \mathbf{D}_{2y} & \eta_2^0 \\ \mathbf{D}_{3x} & \mathbf{D}_{3y} & \eta_3^0 \end{bmatrix} \begin{bmatrix} x \\ y \\ 1 \end{bmatrix} = [\overline{\mathbf{D}}]\ \ \overline{\mathbf{X}} \tag{8}$$

where :

- $\mathbf{D}_i$ is the ith *shape vector* of triangle T_P.
- η_i^0 is the ith barycentric coordinate of the origin of the coordinate frame.

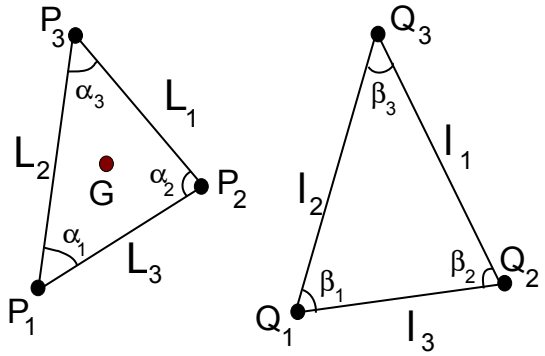

Fig. 5. (Left) Rest triangle T_P whose vertices are $\mathbf{P}_i$; (Right) Deformed triangle whose vertices are $\mathbf{Q}_i$.

Shape vectors $\mathbf{D}_i$ are the gradient vectors of the barycentric coordinates η_i (the shape functions) and they play a key role in the discretization of the membrane energy. Those vectors are directed along the inner normal (independently of the triangle orientation) and are of length $1/h_i$, h_i being the altitude of $\mathbf{P}_i$ (see Figure 6(left)). This can be translated with the following geometric relation :

$$\mathbf{D}_i = \frac{1}{2\mathcal{A}_P}(\mathbf{P}_{i\oplus 1} - \mathbf{P}_{i\oplus 2})^\perp \tag{9}$$

where $i \oplus j = ((i - 1 + j) \bmod 3) + 1$ and $\mathbf{X}^\perp = (-y, x)^T$ is the orthogonal of vector $\mathbf{X}$.

Another important fact is that each pair of shape vectors $(\mathbf{D}_i, \mathbf{D}_j)$ is the covariant basis of the contravariant basis made by the two vectors $(\mathbf{P}_{i+1} - \mathbf{P}_{i+2})$ and $(\mathbf{P}_{j+1} - \mathbf{P}_{j+2})$. Thus, if $i \neq j$ are two distinct indices, and for all vector $\mathbf{a} \in \mathbb{R}^2$, we have the following two relations :

$$\mathbf{a} = (\mathbf{a} \cdot \mathbf{D}_i)(\mathbf{P}_{i\oplus 1} - \mathbf{P}_{i\oplus 2}) + (\mathbf{a} \cdot \mathbf{D}_j)(\mathbf{P}_{j\oplus 1} - \mathbf{P}_{j\oplus 2})$$
$$\mathbf{a} = (\mathbf{a} \cdot (\mathbf{P}_{i\oplus 1} - \mathbf{P}_{i\oplus 2}))\mathbf{D}_i + (\mathbf{a} \cdot (\mathbf{P}_{j\oplus 1} - \mathbf{P}_{j\oplus 2}))\mathbf{D}_j$$

Other remarkable properties of shape vectors are detailed in appendix II but a fundamental result is that all shape vectors sum to zero :

$$\mathbf{D}_1 + \mathbf{D}_2 + \mathbf{D}_3 = \mathbf{0} \tag{10}$$

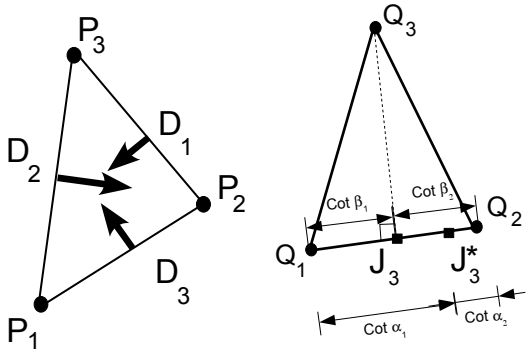

Fig. 6. (Left) Shape vectors $polarv_i$ are orthogonal to each edge and directed inwards; (Right) The foot $\mathbf{J}_i$ is the barycenter of points $\mathbf{Q}_j$ and $\mathbf{Q}_k$ with coefficients $\cot\beta_j$ and $\cot\beta_k$ while pseudo-foot point $\mathbf{J}_i^\star$ has barycentric coordinates $\cot\alpha_j$ and $\cot\alpha_k$.

To simplify notations, we introduce the centroid $\mathbf{G}$ of triangle T_P of barycentric coordinates $\eta_i = 1/3$ in the Equation 7 :

$$\mathbf{X} = \sum_{i=1}^{3} \eta_i(\mathbf{X})\ \mathbf{P}_i = \sum_{i=1}^{3} \left(\frac{1}{3} + \mathbf{D}_i \cdot (\mathbf{X} - \mathbf{G})\right)\ \mathbf{P}_i \quad (11)$$

The deformation function $\mathbf{\Phi}(\mathbf{X})$ on a linear triangle maps a point $\mathbf{X} \in T_P$ such that $\mathbf{\Phi}(\mathbf{X})$ has the same barycentric coordinates in triangle T_Q than $\mathbf{X}$ in triangle T_P :

$$\mathbf{\Phi}(\mathbf{X}) = \sum_{i=1}^{3} \eta_i(\mathbf{X})\ \mathbf{Q}_i = \sum_{i=1}^{3} \left(\frac{1}{3} + \mathbf{D}_i \cdot (\mathbf{X} - \mathbf{G})\right)\ \mathbf{Q}_i \quad (12)$$

C. Invariants of the Green-Lagrange Strain Tensor

To write the total membrane energy $W(T_P)$ necessary to deform triangle T_P into triangle T_Q, it is necessary to write the two invariants $\mathrm{tr}\mathbf{E}$ and $\mathrm{tr}\mathbf{E}^2$ as a function of the two triangles shape. From Equation 12, it can be seen that the gradient of the deformation function is independent is constant on the rest triangle T_P which simplifies further expressions :

$$\nabla\mathbf{\Phi} = \left[\frac{\partial \mathbf{\Phi}_i}{\partial x_j}\right] = \sum_{i=1}^{3} \mathbf{Q}_i \otimes \mathbf{D}_i$$

$$\mathbf{C} = \nabla\mathbf{\Phi}^T \nabla\mathbf{\Phi} = \sum_{i=1}^{3}\sum_{j=1}^{3} (\mathbf{Q}_i \cdot \mathbf{Q}_j)(\mathbf{D}_i \otimes \mathbf{D}_j) \quad (13)$$

The trace of the Green strain tensor $\mathrm{tr}\mathbf{E}$ is simply derived from the trace of the tensor $\mathbf{C}$: $\mathrm{tr}\mathbf{E} = 1/2(\mathrm{tr}\mathbf{C} - 2)$. From equation 13, we easily get :

$$\mathrm{tr}\mathbf{C} = \sum_{i=1}^{3}\sum_{j=1}^{3} (\mathbf{Q}_i \cdot \mathbf{Q}_j)(\mathbf{D}_i \cdot \mathbf{D}_j) \quad (14)$$

Appendix III details how this sum of dot products can be expressed as a function of edge length and angles. The resulting expressions are simply :

$$\mathrm{tr}\mathbf{C} = \frac{1}{2\mathcal{A}_P}\left(l_1^2 \cot\alpha_1 + l_2^2 \cot\alpha_2 + l_3^2 \cot\alpha_3\right)$$

$$\mathrm{tr}\mathbf{E} = \frac{(l_1^2 - L_1^2)\cot\alpha_1 + (l_2^2 - L_2^2)\cot\alpha_2 + (l_3^2 - L_3^2)\cot\alpha_3}{2\mathcal{A}_P}$$

The expression of $\mathrm{tr}\mathbf{C}$ is closely related to the Dirichlet energy used in discrete harmonic mapping [33]. Indeed, in this case, the deformation $\mathbf{\Phi}$ maps two planar surfaces and the right Cauchy-Green deformation tensor is just the first fundamental form and its trace the norm of the deformation matrix : $\mathrm{tr}\mathbf{C} = \|\nabla\mathbf{\Phi}\|^2$. Extending the analogy with the field of surface parametrization, we can see the membrane energy as a functional that enforces isometric mappings (instead of conformal or harmonic ones) since it is minimal when $\mathbf{C} = \mathbf{I}$.

The second invariant of the strain tensor $\mathrm{tr}\mathbf{E}^2$ can be written as a function of the first invariant and the determinant of $\mathbf{E}$ but also of $\mathbf{C}$:

$$\mathrm{tr}\mathbf{E}^2 = (\mathrm{tr}\mathbf{E})^2 - 2\det\mathbf{E} = \frac{1 + 2\mathrm{tr}\mathbf{E} + 2(\mathrm{tr}\mathbf{E})^2 - \det\mathbf{C}}{2}$$

The determinant of the deformation tensor $\mathbf{C} = \nabla\mathbf{\Phi}^T\nabla\mathbf{\Phi}$ is the square of the determinant of $\mathbf{\Phi}$ which is the ratio of the two triangle areas : $\det\mathbf{\Phi} = \mathcal{A}_Q/\mathcal{A}_P$. Putting it all together, the second invariant is also a simple function of the square edge elongation $\Delta^2 l_i = (l_i^2 - L_i^2)$

$$\mathrm{tr}\mathbf{E}^2 = \frac{\sum_{i\neq j} 2\Delta^2 l_i \Delta^2 l_j - \sum_{i=1}^{3}(\Delta^2 l_i)^2}{64\mathcal{A}_P^2}$$

D. Membrane Energy and Triangular Biquadratic Springs

The density of elastic energy $W(\mathbf{X})$ is given by Equation 6 and is constant for all points in triangle T_P. Thus, from previous results, we can show that the total energy to deform triangle T_P into T_Q is a function of square edge variation $\Delta^2 l_i$ and of the angles α_i of the rest triangle :

$$W_{TRBS}(T_P) = \int_{T_P} W(\mathbf{X})\ d\mathbf{X} = \mathcal{A}_P W(\mathbf{G})$$

$$W_{TRBS}(T_P) = \sum_{i=1}^{3} \frac{(\Delta^2 l_i)^2(2\cot^2\alpha_i(\lambda+\mu)+\mu)}{64\mathcal{A}_P} + \sum_{i\neq j} \frac{2\Delta^2 l_i \Delta^2 l_j (2\cot\alpha_i\cot\alpha_j(\lambda+\mu)-\mu)}{64\mathcal{A}_P} \quad (15)$$

We call this formulation of the membrane energy the *TRiangular Biquadratic Springs* (TRBS) since the first term can be interpreted as the energy of three *tensile biquadratic springs* that prevent edges from stretching while the second term can be seen as three *angular biquadratic springs* that prevent any change in vertex angles. We can thus rewrite the previous equation by enforcing the existence of those two types of biquadratic springs :

$$W_{TRBS}(T_P) = \sum_{i=1}^{3} \frac{k_i^{T_P}}{4}(l_i^2 - L_i^2)^2 + \sum_{i\neq j} \frac{c_k^{T_P}}{2}(l_i^2 - L_i^2)(l_j^2 - L_j^2)$$

where k_{T_P} and c_{T_P} are the tensile and angular stiffness of the biquadratic springs. Replacing the Lamé coefficients with the Young modulus E and Poisson coefficient ν, we get :

$$k_i^{T_P} = \frac{2\cot^2\alpha_i(\lambda+\mu)+\mu}{16\mathcal{A}_P} = \frac{E(2\cot^2\alpha_i + 1 - \nu)}{16(1-\nu^2)\mathcal{A}_P}$$

$$c_k^{T_P} = \frac{2\cot\alpha_i\cot\alpha_j(\lambda+\mu)-\mu}{16\mathcal{A}_P} = \frac{E(2\cot\alpha_i\cot\alpha_j + \nu - 1)}{16(1-\nu^2)\mathcal{A}_P}$$

The tensile stiffness is always positive while the angular stiffness may be null or even negative. In Figure 7, normalized values of the tensile and angular stiffness are displayed as a function of the Poisson ratio. To this end, all triangles are assumed to be regular $\alpha_i = \pi/3$, to have unit area $\mathcal{A}_P = 1$ and unit Young modulus $E = 1$. It is remarkable to note that for $\nu = 1/3$ the tensile stiffness is minimum and the angular stiffness is zero, the angular stiffness being negative for small Poisson ratio $\nu < 1/3$. When the Poisson ratio approaches 1, the material becomes more and more incompressible and both stiffness sharply increases toward infinity.

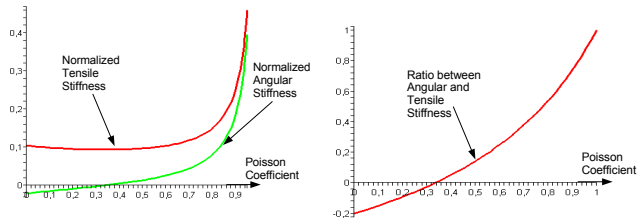

Fig. 7. (Left) Plot of the normalized tensile and angular stiffness as a function of the Poisson ratio; (Right) Ratio c^{T_P}/k^{T_P} as a function of the Poisson ratio.

The membrane energy to deform the whole triangulation Ω_h is simply the sum of the energies of each triangle $T_P \in \Omega_h$. Thus, if an edge is shared by two triangles $T1$ and $T2$, the total tensile stiffness of that edge k_T will be the sum of the two stiffnesses :$k^T = k^{T1} + k^{T2}$. If a triangle has p triangles and e edges, the membrane energy can be decomposed into $3p$ angular biquadratic springs and e tensile biquadratic springs.

E. Force and Stiffness Computation

Applying the Rayleigh-Ritz analysis, we consider that the triangular surface should evolve by minimizing its membrane energy, therefore along the opposite derivative of that energy with respect to the nodes of the system, *i.e.* the deformed positions $\mathbf{Q}_i$. :

$$\mathbf{F}_i^{TRBS}(T_P) = -\left(\frac{\partial W(T_P)}{\partial \mathbf{Q}_i}\right)^T = \sum_{j\neq i} k_k^{T_P}\Delta^2 l_k(\mathbf{Q}_j - \mathbf{Q}_i) + \sum_{j\neq i}(c_j^{T_P}\Delta^2 l_i + c_i^{T_P}\Delta^2 l_j)(\mathbf{Q}_j - \mathbf{Q}_i) \quad (16)$$

We can provide a geometric interpretation of that force, if we consider the two points $\mathbf{J}_i$ and $\mathbf{J}_i^\star$ in the deformed triangle T_Q. The first point $\mathbf{J}_i$ is the foot of $\mathbf{Q}_i$ also defined as the barycenter of points $\mathbf{Q}_j$ and $\mathbf{Q}_k$ with coefficients $\cot\beta_j$ and $\cot\beta_k$. The second point $\mathbf{J}_i^\star$ is a pseudo-foot point defined as the barycenter of points $\mathbf{Q}_j$ and $\mathbf{Q}_k$ with coefficients $\cot\alpha_j$ and $\cot\alpha_k$ (see Figure 6(right)). With those two additional points, the force can be written as :

$$\mathbf{F}_i^{TRBS}(T_P) = \frac{(\lambda+\mu)l_i^2 \mathrm{tr}\mathbf{E}}{4\mathcal{A}_P}(\mathbf{Q}_i - \mathbf{J}_i^\star) + \frac{\mu}{8\mathcal{A}_P}\left(l_i^2(\mathbf{Q}_i - \mathbf{J}_i^\star) - L_i^2(\mathbf{Q}_i - \mathbf{J}_i)\right)$$

The force is clear zero if $T_Q = T_P$ since we then have $\mathrm{tr}\mathbf{E} = 0$ and $\mathbf{J}_i^\star = \mathbf{J}_i$. It is also important to note that if the rest triangle T_P is obtuse in α_j or α_k then the point $\mathbf{J}_i^\star$ is not in the segment $[\mathbf{Q}_j, \mathbf{Q}_k]$ which can be the cause of instabilities.

The tangent stiffness matrix $[\mathbf{B}_{ij}^{TRBS}]$ is a 3×3 matrix (in general not symmetric but with $[\mathbf{B}_{ij}^{TRBS}] = [\mathbf{B}_{ji}^{TRBS}]^T$) that describes how the elastic force varies with respect to an adjacent node position :

$$[\mathbf{B}_{ij}^{TRBS}] = -\frac{\partial W_P}{\partial \mathbf{Q}_i \partial \mathbf{Q}_j} = \frac{\partial \mathbf{F}_i^{TRBS}}{\partial \mathbf{Q}_j}$$

Furthermore, the translation invariance implies that the diagonal stiffness matrix $[\mathbf{B}_{ii}^{TRBS}]$ is the opposite of the sum of the off-diagonal stiffness matrices $[\mathbf{B}_{ij}^{TRBS}]$, $i \neq j$. Expanding the stiffness coefficients, we get the following expression, for $k \neq i, j$:

$$[\mathbf{B}_{ij}^{TRBS}] = (\kappa_k^{T_P}\ \Delta^2 l_k + c_j^{T_P}\ \Delta^2 l_i + c_i^{T_P}\ \Delta^2 l_j)\mathbf{I} + 2c_k^{T_P}(\mathbf{Q}_i - \mathbf{Q}_k)\otimes(\mathbf{Q}_k - \mathbf{Q}_j) + 2c_i^{T_P}(\mathbf{Q}_i - \mathbf{Q}_k)\otimes(\mathbf{Q}_i - \mathbf{Q}_j) + 2c_j^{T_P}(\mathbf{Q}_j - \mathbf{Q}_i)\otimes(\mathbf{Q}_j - \mathbf{Q}_k) + 2k_k^{T_P}(\mathbf{Q}_i - \mathbf{Q}_j)\otimes(\mathbf{Q}_i - \mathbf{Q}_j) \quad (17)$$

F. Stress Tensors and law of motion

In finite strain mechanics there are different definition of stress tensors depending if it is expressed in the reference or the deformed configuration. The second Piola-Kirchhoff for instance is a symmetric tensor defined as the energy conjugate of the strain tensor $\mathbf{S} = \partial W/\partial \mathbf{E}$. Because we use a linear material, this stress tensor is proportional to the strain tensor :$\mathbf{S} = \lambda(\mathrm{tr}\mathbf{E})\mathbf{I} + \mu\mathbf{E}$.

The Cauchy or true stress tensor $\mathbf{\Sigma}$ represents the force per unit area of the deformed solid $\mathbf{\Sigma} = (\mathcal{A}_Q/\mathcal{A}_P)(\nabla\mathbf{\Phi}\mathbf{S}\nabla\mathbf{\Phi}^T)$. The first Piola-Kirchhoff or nominal stress tensor $\mathbf{T}$ is the energy conjugate of the deformation gradient and is simply related with the second Piola-Kirchhoff stress $\mathbf{T} = \nabla\mathbf{\Phi}\ \mathbf{S}$.

All those tensors are constant along the triangle T_P and the nodal force $\mathbf{F}_i^{TRBS}$ defined in the previous section is related to the first Piola-Kirchhoff stress tensor : $\mathbf{F}_i^{TRBS} = -\mathcal{A}_P\mathbf{T}\mathbf{D}_i$ (see proof in appendix IV).

The law of motion is given by the conservation of linear momentum, which can be written in the reference configuration with the divergence of tensor $\mathbf{T}$:

$$\nabla\cdot\mathbf{T} + \rho\mathbf{R}^g(\mathbf{X}) = \rho\frac{d^2\mathbf{\Phi}(\mathbf{X})}{dt^2} \quad (18)$$

where ρ is the mass density and $\mathbf{R}^g(\mathbf{X})$ a density of body forces (typically a gravity force). To obtain the elastic, body and acceleration forces at nodal points $\mathbf{Q}_i$, it is necessary to obtain the *weak form* of Equation 18 for instance by invoking the principle of virtual work and to use shape functions $\eta_i(\mathbf{X})$ as the test functions [31] (see Appendix IV for proof). If the mass matrix is further constrained to be diagonal (mass lumping), we then get the law of motion for the node i :

$$\sum_{T_P\in\mathcal{S}_P}\mathbf{F}_i^{TRBS}(T_P) + \mathbf{R}^b = m_i\frac{d\mathbf{Q}_i}{dt^2} \quad (19)$$

IV. Approximation of the membrane energy

A. Small Displacements : Linear Elastic Membrane

We propose a first approximation of the membrane energy in the case of small displacements, corresponding to the framework of linear elasticity. In such case, it is preferable to analyze the deformation of a membrane surface in terms of displacement $\mathbf{u}(\mathbf{X}) = \mathbf{\Phi}(\mathbf{X}) - \mathbf{X}$ rather than in terms of deformation $\mathbf{\Phi}(\mathbf{X})$. The linear elastic membrane energy is derived by replacing the Green-Lagrange strain tensor with its linearized version : $\mathbf{E}_{\mathrm{L}} = \frac{1}{2}(\nabla\mathbf{u} + \nabla\mathbf{u}^T)$.

On a linear triangle element, the linear membrane energy is a quadratic expression of the displacements $\mathbf{u}_i$ of the three vertices (see [6] for an equivalent expression of the local stiffness matrix) :

$$W_L(T_P) = \frac{1}{2}\sum_{i,j=0}^{3} \mathbf{u}_i^T[\mathbf{B}_{ij}^L]\mathbf{u}_j$$

$$[\mathbf{B}_{ij}^L] = \Big[\lambda(\mathbf{D}_i \otimes \mathbf{D}_j) + \frac{\mu}{2}(\mathbf{D}_j \otimes \mathbf{D}_i) + \frac{\mu}{2}(\mathbf{D}_i \cdot \mathbf{D}_j)\mathbf{I}\Big]$$

The linear elastic approximation is advantageous in terms of computational efficiency (see section V-A) since the elastic force can be evaluated by a simple matrix vector computation which is why it has been coined as a Tensor-Mass approach [29]. However it is quite restrictive in practice with the occurrence of exaggerated dilation when large rotations are applied [34]. Note that when $\mathbf{Q}_i = \mathbf{P}_i$, the TRBS tangent stiffness matrix of Equation 17 is equal to the linear elastic stiffness matrix.

B. Small Deformations : Triangular Quadratic Springs

A second simplification of the TRBS energy can be done by considering that the amount of deformation of deformed triangle T_Q is small, *i.e.* edge lengths l_i of T_Q are close to rest lengths L_i. With this hypothesis, the square edge elongation $\Delta^2 l_i = (l_i^2 - L_i^2)$ can be simplified as $\Delta^2 l_i \approx 2L_i(l_i - L_i)$. Writing the edge elongation as $dl_i = l_i - L_i$, we can define the *TRiangular Quadratic Springs* (TRQS) as an approximation of TRBS :

$$W_{TRQS}(T_P) = \sum_{i=1}^{3} \frac{1}{2}\kappa_i^{T_P}(dl_i)^2 + \sum_{i\neq j} \gamma_k^{T_P} dl_i dl_j \tag{20}$$

$$\kappa_i^{T_P} = 2L_i^2 k_i^{T_P} = \frac{L_i^2(2\cot^2\alpha_i(\lambda+\mu)+\mu)}{8\mathcal{A}_P} \tag{21}$$

$$\gamma_k^{T_P} = 2L_iL_jc_k^{T_P} = \frac{L_iL_j(2\cot\alpha_i\cot\alpha_j(\lambda+\mu)-\mu)}{8\mathcal{A}_P}$$

Thus by adding angular springs to the regular (tensile) spring-mass models, largely used in the computer graphics community, and by carefully choosing their stiffness parameters, one can propose a deformable model which is an approximation of a hyperelastic model derived from continuum mechanics. To the best of our knowledge, it is the first time that a theoretical link between spring-mass models and continuum mechanics is established. Without the addition of angular springs, mass springs models with the right stiffness parameters can at best approximate the behavior of a membrane with $\nu = 1/3$ (see [35] for a similar conclusion based on linear elasticity analogy). With angular springs, the TRQS model is equivalent to the TRBS model, a isotropic membrane energy for a linear material, but only for small deformations of triangles : $dl_i/L_i < 10\%$. However, it is important to stress that a TRQS model *is not a model based on continuum mechanics* since its energy $W_{TRQS}(T_P)$ is not a function of the two strain invariants $tr\mathbf{E}$ and $tr\mathbf{E}^2$. This implies that for large displacements, the behaviour of TRQS models may depend on the geometry and topology of the mesh and not only on the material properties.

There has been several previous attempts to compare spring mass models with continuum mechanics. Van Gelder [6] has previously proposed to estimate the equivalent stiffness of a spring mass model by comparing the stiffness matrix of a linear elastic triangle with that of a spring mass model. His estimation of the stiffness coefficient $\kappa_i^{T_P} = E/2(1-\nu^2)(2\mathcal{A}_P(1-\nu)/L_i^2 + \nu\cot\alpha_i)$ significantly differs from Equation 21 and it has been shown by Baudet [36] that the behaviour of such membrane models is not correct.

A major limitation in those attempts to identify the stiffness parameters of spring-mass models from FEM models has been to exclude angular springs. Indeed, the level of material compressibility (controlled by ν) can only be modified independently of the material stiffness (controlled by E) with the addition of angular springs. Because of this limitation, authors [36], [37] have often turned to the estimation of spring stiffness of quadrilateral elements, because it was possible to add "shear springs" along their diagonals.

The elastic force of TRQS is computed by computing the derivative of the TRQS energy with respect to the node position $\mathbf{Q}_i$:

$$\mathbf{F}_i^{TRQS}(T_P) = -\frac{\partial\tilde{W}_{TRQS}(T_P)}{\partial\mathbf{Q}_i} = \sum_{j\neq i}\kappa_j^{T_P}(dl_j)\frac{\mathbf{Q}_k-\mathbf{Q}_i}{l_j} +$$

$$\sum_{j\neq i}(\gamma_k^{T_P}dl_i + \gamma_i^{T_P}dl_k)\frac{\mathbf{Q}_k-\mathbf{Q}_i}{l_j}$$

Similarly the tangent stiffness matrix is computed as :

$$-\frac{\partial\tilde{W}_P}{\partial\mathbf{Q}_i\partial\mathbf{Q}_j} = \frac{\kappa_k^{T_P}\ dl_k + \gamma_j^{T_P}\ dl_i + \gamma_i^{T_P}\ dl_j}{l_k}\mathbf{I} +$$

$$\frac{\gamma_k^{T_P}}{l_il_j}(\mathbf{Q}_k-\mathbf{Q}_i)\otimes(\mathbf{Q}_j-\mathbf{Q}_k) +$$

$$\frac{\gamma_i^{T_P}}{l_jl_k}(\mathbf{Q}_i-\mathbf{Q}_k)\otimes(\mathbf{Q}_i-\mathbf{Q}_j) +$$

$$\frac{\gamma_j^{T_P}}{l_il_k}(\mathbf{Q}_j-\mathbf{Q}_i)\otimes(\mathbf{Q}_j-\mathbf{Q}_k) +$$

$$\frac{\kappa_k^{T_P}\ L_k - \gamma_j^{T_P}\ dl_i - \gamma_i^{T_P}\ dl_j}{l_k^3}(\mathbf{Q}_i-\mathbf{Q}_j)\otimes(\mathbf{Q}_i-\mathbf{Q}_j)$$

V. Implementation and Results

A. Comparison of Execution time

We have implemented four different elastic membrane formulations in the SOFA platform[1] to benchmark their performance. Those formulations include the linear elastic membrane, the TRQS and TRBS membranes as well a regular

[1]SOFA is an open source medical simulation platform available at www.sofa-framework.org

spring-mass membrane obtained by dropping the angular springs in the TRQS formulation.

To optimize the execution time of the TRBS and TRQS membrane forces, the tensile stiffness $\kappa_i^{T_P}$ and $k_i^{T_P}$ are stored on edges and are accumulated from adjacent triangles. Thus, the force computation first requires to examine all edges to compute their extensions ($\Delta^2 l_i$ and dl_i) and the tensile terms followed by the examination of all triangles to add the angular terms. In the latter case, each edge term may be computed only once by taking advantage of the action-reaction principle ($\mathbf{F}_{i\to j} = -\mathbf{F}_{j\to i}$).

In section III-F we have showed that the application of the regular finite element or finite volume method (such as [38]) is equivalent to the TRBS membrane but with a formulation of the force which involves the first Piola-Kirchhoff tensor :$\mathbf{F}_i^{TRBS} = -\mathcal{A}_P \mathbf{T}\mathbf{D}_i$. The computation of the membrane forces for the three vertices of a tridimensional triangle based on FEM requires 121 multiplications and 75 additions while the TRBS forces can be computed with 30 multiplications and 44 additions[2] which represents at least a speedup factor of two. Thus, the biquadratic spring formulation performs an optimal assembly of the stiffness information.

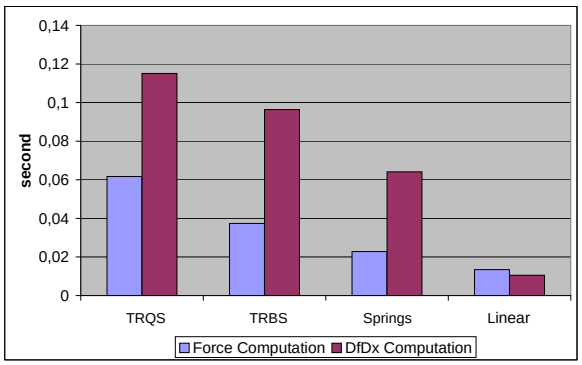

Fig. 8. Execution times to compute 100 times the elastic force $\mathbf{F}_i$ and the matrix-vector product $[\mathbf{B}_{ij}]\mathbf{X}$ for 4 differents elastic membrane formulations.

In Figure 8, we compare the execution times for the evaluation of the elastic membrane force $\mathbf{F}_i$ as well as the matrix-vector product $[\mathbf{B}_{ij}]\mathbf{X}$ on a triangular mesh having 774 vertices and 1546 triangles. The matrix-vector product evaluation is useful to benchmark the performance of the conjugated gradient algorithm. The linear elastic membrane is the most efficient, followed by the spring-mass, TRBS and TRQS models. The TRBS is only 60% more expensive than the spring-mass, while the TRBS is itself 60 % more expensive than the TRQS. The execution times for the matrix-vector products follow the same hierarchy but with smaller differences between the models (the TRQS is only 20% more expensive than the TRBS in this case).

[2]The decomposition of forces based on FEM exploits the fact that all nodal forces of a triangle sum to zero $\mathbf{F}_i + \mathbf{F}_j + \mathbf{F}_k = 0$. In the case of TRBS, we have assumed that each edge is shared by two triangles.

B. Comparison on test cases

We compare the behavior of the four membrane formulations in a pure traction study for which there is a known analytical solution for linear elastic materials. Figure 9 summarizes the boundary conditions consisting in applying a known pressure p on the top of a square membrane while preventing the vertical displacements of the bottom vertices. In the linear elastic case, the vertical and horizontal strains, ϵ_y and ϵ_x are proportional to the applied pressure : $\epsilon_y = E\ p$ and $\epsilon_x = E\ \nu\ p$.

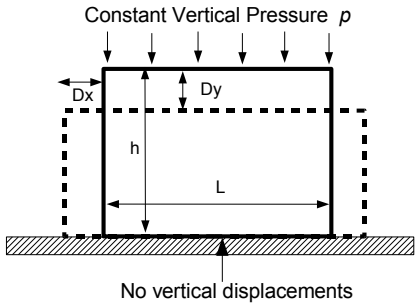

Fig. 9. Pure traction experiment where a constant pressure is applied on a slab, bottom vertices being constrained to have zero vertical displacements. The horizontal and vertical deformations are computed as $\epsilon_x = Dx/L$ and $\epsilon_y = Dy/h$.

Several indentation tests have been performed on a membrane material having unit Young Modulus $E = 1$ and varying Poisson ratios $\nu \in [0, 1[$. We solve those non-linear static problems with an implicit method, using the tangent stiffness matrices (Newton-Raphson algorithm), each linear system of equations being solved with the modified conjugated gradient of Baraff and Witkin [14]. In Figure 10, the curves $p(\epsilon_y) \approx E\epsilon_y$ and $\epsilon_x(\epsilon_y) \approx -\nu\epsilon_y$ are displayed for the linear and the TRBS membranes for a given Poisson ratio $\nu = 0.6$. Those curves have been computed from the mesh of Figure 12 (a). As expected, all curves are linear for small strains while the TRBS membrane leaves the domain of linearity for strain greater than 3%. For extensions, $p > 0$, TRBS membranes exhibit a greater stiffness than linear membranes while the converse is true for compressions. The differences in the stress-strain relationships can be readily explained by the difference between the Green-Lagrange strain (quadratic function of stretch) used in the TRBS model and the engineering strain (linear function of stretch) for the linear model. Indeed, the curves $p(\epsilon_y)$ closely resemble that of the curves dw_B/ds in Figure 3.

For a strong compression, $p = -0.1$, away from the linear domain $\epsilon_x \approx 10\%$, the TRBS membrane exhibits vertical strains that are on average 20% greater than in the linear case (see Figure 11). The TRQS membrane has a intermediate behavior between the linear and TRBS membranes which is sensible since it is a large displacement formulation (as the TRBS case) but with a strain measure (engineering strain) similar to linear materials. Finally using tensile springs leads to solutions that are far from being physical except when the Poisson ratio is close to 0.3, which correlates the findings of section III-D.

The impact of the mesh homogeneity on the computed

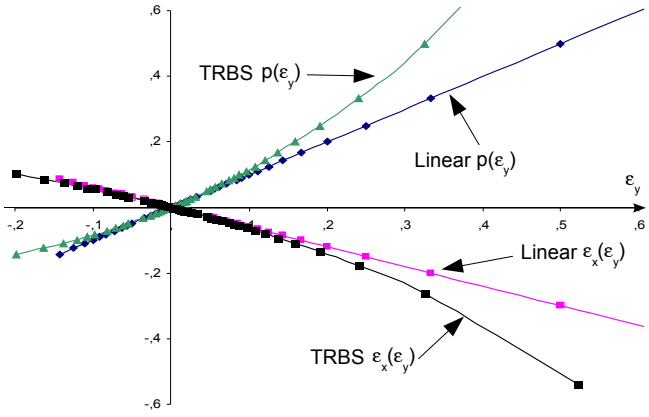

Fig. 10. Curves $p(\epsilon_y)$ and $\epsilon_x(\epsilon_y)$ for pure traction experiments with TRBS and linear membranes ($\nu = 0.6$)

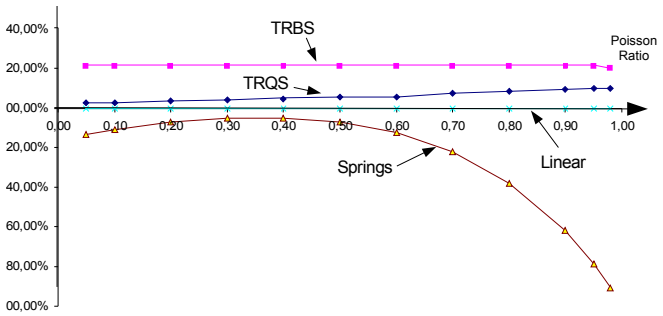

Fig. 11. Graphs of the relative difference between the computed vertical strain and the theoretical linear strain $(\epsilon_y - \epsilon_y^{Lin})/\epsilon_y^{Lin}$ for a strong compression $p = -0.1$ and for a large range of Poisson ratios.

deformation has been tested by comparing the deformations produced by the TRBS membrane on the two meshes displayed in Figure 12. The computed strains were actually very close to each other with a relative difference between strains less than 5% (with an average of 1.1%) for the same applied pressures. Similar results were obtained with the TRQS elastic membrane but with a greater discrepancy (average of 2.54%). The relative independence of behavior of TRBS with respect to mesh resolution and homogeneity is theoretically guaranteed because, unlike the TRQS, it is based on continuum mechanics. Although additional tests should be performed, the triangular quadratic springs (TRQS) seems to be also quite insensitive to the mesh topology. Therefore, TRBS and TRQS are very well suited for multigrid [39] or multi-resolution [28], [40] approaches.

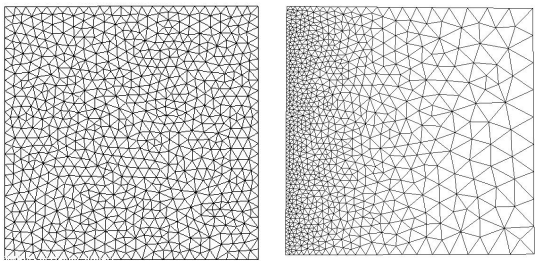

(a) (b)

Fig. 12. Two square meshes on which the pure traction experiments have been performed. The rightmost triangular mesh has a strong variation of triangle sizes while the leftmost one is more uniform.

C. Cloth Animation

We simulate below the deformation of a tablecloth under the effect of gravity forces. To this end, we add to the Newtonian law of motion of Equation 19, bending and damping forces. For bending, we use the damped formulation of Bridson [24] *et al.* because it makes bending forces "orthogonal" to membranes (tangential) forces. To damp membrane forces, it is very common in Finite Element analysis to consider a damping matrix proportional to the mass and stiffness matrices (Rayleigh damping [41]).

To optimize computation, we propose in the TRBS case, to replace the square elongation $\Delta^2 l_i$ with its damped value in equation 16 :

$$(\Delta^2 l_i)^{\text{Damped}} = \Delta^2 l_i + \zeta(\mathbf{v}_j - \mathbf{v}_k) \cdot (\mathbf{Q}_j - \mathbf{Q}_k)$$

ζ being the damping coefficient and $\mathbf{v}_j$ being the speed of vertex j. This simple approach is equivalent to considering a local damping matrix proportional to a modified local stiffness matrix where the terms proportional to the identity matrix in Equation 17 have been dropped. It is important to note that, in this case, the final damping matrix is still invariant with respect to global rotations. Similarly, for the TRQS case, we replace the edge elongation dl_i with its damped value :

$$(dl_i)^{\text{Damped}} = dl_i + \zeta(\mathbf{v}_j - \mathbf{v}_k) \cdot \frac{(\mathbf{Q}_j - \mathbf{Q}_k)}{\|\mathbf{Q}_j - \mathbf{Q}_k\|}$$

The time integration of the law of motion is based on a backward Euler method with membrane forces being integrated implicitly. Linear equations are solved with a conjugated gradient algorithm with no preconditioning. Simulations of a tablecloth falling lying on a table are shown in Figure 13 for various choices of membranes and Poisson ratios. Those experiments are based on the mesh of Figure 10 (a) with mass lumping, bending forces set to 0.05 and Young modulus set to 200. The computation time is around 3s on a

Using a nearly incompressible material $\nu = 0.95$ for both TRBS and TRQS results in fairly regular folds, while for low Poisson ratios the number and the shape folds tends to be much less regular. For $\nu = 0.95$, the TRBS and TRQS membranes behave very closely while for low Poisson ratios the amplitude of the folds is greater when the TRQS membrane is employed. As expected, using tensile springs only with $\nu = 0.3$ results in a shape which is fairly close to the TRQS with low Poisson ratio.

VI. Conclusion

In this paper, we have first showed that tensile quadratic and biquadratic springs correspond to a finite element discretization of stretching energy on curves for two different choices of strain functions, the engineering strain and Green-Lagrange strain. In the two-dimensional case, two new non-linear membrane formulations have been introduced: the triangular biquadratic and quadratic springs. The TRBS is equivalent to a finite strain membrane material with a linear stress-strain relation (St Venant-Kirchhoff membrane) when the discretization is based on linear triangle elements and the finite element method (see Figure 14). This set of tensile

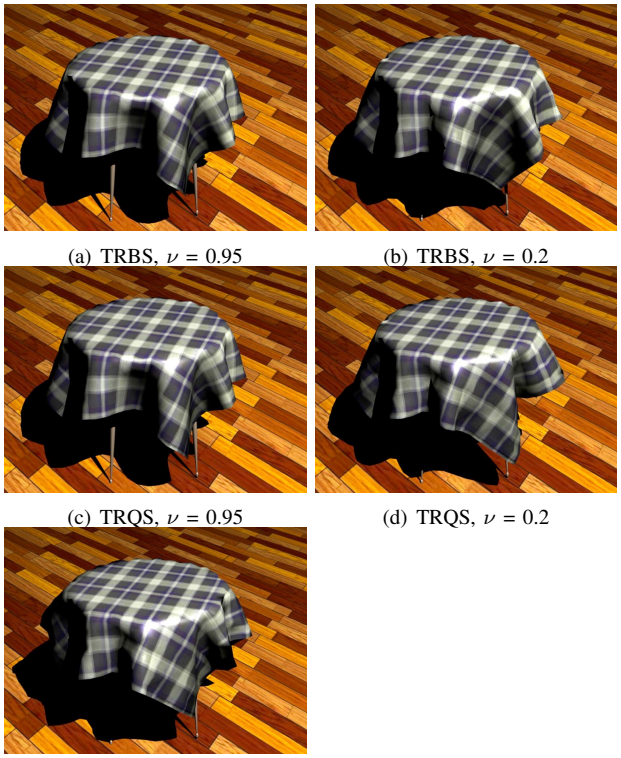

(a) TRBS, ν = 0.95 (b) TRBS, ν = 0.2

(c) TRQS, ν = 0.95 (d) TRQS, ν = 0.2

(e) Springs, ν = 0.3

Fig. 13. Comparison between different membrane models of a tablecloth lying on a table.

and angular biquadratic springs leads to efficient computations (only 60 % more costly than springs). The TRQS membranes are approximations of the TRBS for small deformations and can also be decomposed into tensile quadratic springs (corresponding to regular springs) and angular quadratic springs. TRBS are not isotropic hyperelastic materials since their strain energy do not depend on the strain invariants. But they can be considered as asymptotically hyperelastic in the same way than linear elastic materials are asymptotically hyperelastic for small displacements. Finally, it has been showed that for Poisson ratio $\nu = 0.3$, the angular springs may be neglected and, in such case, regular mass-springs models can be used to approximate TRQS membranes.

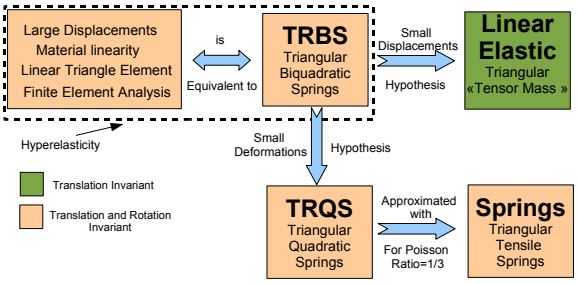

Fig. 14. Relations between the introduced membrane formulations : TRBS, TRQS and springs.

Thus, we have established a formal link between springs, widely use in computer graphics, and continuum mechanics through the introduction of biquadratic springs. Furthermore, as shown in III-C, any isotropic isotropic hyperelastic membrane can be expressed as a function of the two invariants of the strain tensor and therefore can be expressed in terms of tensile and angular biquadratic springs.

This study on springs and continuum mechanics should be extended in several directions, for instance to other planar finite elements such as quads, to the case of three-dimensional elastic materials discretized with tetrahedral or hexahedral meshes or to describe anisotropic materials, especially in the context of cloth or biomechanical modeling.

Appendix I
Basic Triangle trigonometry

Three important trigonometric relations in triangle T_P are :

- Cosine Law : $L_i^2 = L_j^2 + L_k^2 - 2L_jL_k\cos\alpha_i$
- Sine Law : $L_i/\sin\alpha_i = 2R_p = (L_1L_2L_3)/(2\mathcal{A}_P)$ where R_p is the radius of the circumscribed circle. Combined with the law of cosine, we get : $\cot\alpha_i = (-L_i^2 + L_j^2 + L_k^2)/(4\mathcal{A}_P)$
- Heron's Formula : $\mathcal{A}_P = \frac{1}{4}\left(L_1^2\cot\alpha_1 + L_2^2\cot\alpha_2 + L_3^2\cot\alpha_3\right)$

Appendix II
On shape vectors

From equations 7 and 8, we can state that $[\overline{\mathbf{D}}]\ [\overline{\mathbf{P}}] = [\overline{\mathbf{P}}]\ [\overline{\mathbf{D}}] = \mathbf{I}$ which leads to the following relations :

$$\sum_i \mathbf{D}_i = 0 \qquad (\mathbf{P}_i - \mathbf{P}_j)\cdot\mathbf{D}_k = 0$$

$$\sum_i \mathbf{D}_i\cdot\mathbf{P}_i = 2 \qquad \sum_i \mathbf{D}_i\cdot\mathbf{P}_{i+1} = -1$$

A shape vector is also related to the derivative of the log triangle area with respect to a vertex position :

$$\mathbf{D}_i = \left(\frac{\partial \log\mathcal{A}_P}{\partial\mathbf{P}_i}\right)^T$$

As such it is simply related with the area vector $\mathbf{S}_i = \mathcal{A}_P\mathbf{D}_i = (\frac{\partial\mathcal{A}_P}{\partial\mathbf{P}_i})^T$ which appears in several publications on geometry processing [42]. To compute shape vectors on tridimensional triangles, it is convenient to use the formula below which does not require to compute the normal vector :

$$\mathbf{D}_i = \frac{1}{2\mathcal{A}_P}\left((\mathbf{P}_i - \mathbf{P}_j)\cot\alpha_k + (\mathbf{P}_i - \mathbf{P}_k)\cot\alpha_j\right)$$

Appendix III
Computation of the trace of $\mathbf{C}$

Shape vectors being orthogonal to each triangle edge (according to Equation 9), their dot product is given as :

$$\text{If } i\neq j,,k\neq i,j\ \ \mathbf{D}_i\cdot\mathbf{D}_j = -\frac{\cot\alpha_k}{2\mathcal{A}_P}\ \text{ If } i=j, \|\mathbf{D}_i\|^2 = \frac{L_i^2}{4\mathcal{A}_P^2}$$

To estimate the dot products between deformed positions $(\mathbf{Q}_i\cdot\mathbf{Q}_j)$, it should be noticed that $tr\mathbf{C}$ is translation invariant (since $\sum_i\mathbf{D}_i = \mathbf{0}$) and therefore it is convenient to choose the origin as the center $\mathbf{O}_Q$ of the circumscribed circle of radius R_Q (see Figure 15). With this choice, we get :

$$\text{If } i\neq j, k\neq i,j\ \ \mathbf{Q}_i\cdot\mathbf{Q}_j = R_Q^2 - \frac{l_k^2}{2}\ \text{ If } i=j, \|\mathbf{Q}_i\|^2 = R_Q^2$$

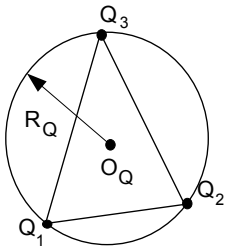

Fig. 15. Definition of the circumscribed circle at triangle T_Q of center $\mathbf{O}_Q$ and radius R_Q.

Combining the two previous equations with Equation 13 :

$$\begin{aligned}
tr\mathbf{C} &= R_Q^2 \sum_{i=1}^{3}\sum_{j=1}^{3}(\mathbf{D}_i \cdot \mathbf{D}_j) + \sum_{i=1}^{3}\sum_{j\neq i}\frac{\cot\alpha_k}{2\mathcal{A}_P}\frac{(l_k)^2}{2} \\
tr\mathbf{C} &= \frac{1}{2\mathcal{A}_P}\sum_{i=1}^{2}\sum_{j>i}\cot\alpha_k l_k^2 \\
tr\mathbf{C} &= \frac{1}{2\mathcal{A}_P}\left(l_1^2\cot\alpha_1 + l_2^2\cot\alpha_2 + l_3^2\cot\alpha_3\right) \qquad (22)
\end{aligned}$$

Appendix IV
Deriving the Law of Motion

First, a relation between the energy gradient and the second Piola Kirchhoff stress tensor $\mathbf{S}$ is derived from the chain rule of derivation :

$$\frac{\partial W_P}{\partial \mathbf{Q}_i} = \frac{\partial W_P}{\partial \mathbf{E}}\frac{\partial \mathbf{E}}{\partial \mathbf{Q}_i} = \mathcal{A}_P\mathbf{S}\frac{\partial \mathbf{E}}{\partial \mathbf{Q}_i}$$

Note that $\frac{\partial \mathbf{E}}{\partial \mathbf{Q}_i}$ is a third order tensor. To simplify the computation, we first look at the first component of the energy gradient $\frac{\partial W_P}{\partial \mathbf{Q}_i^x}$:

$$\frac{\partial W_P}{\partial \mathbf{Q}_i^x} = \mathcal{A}_P\mathbf{S} : \frac{\partial \mathbf{E}}{\partial \mathbf{Q}_i^x} = \frac{\mathcal{A}_P}{2}\mathbf{S} : \frac{\partial \mathbf{C}}{\partial \mathbf{Q}_i^x}$$

where $\mathbf{A} : \mathbf{B} = tr(B^T A)$ is the inner product of the two matrices.

We can further derive the matrix $\frac{\partial \mathbf{C}}{\partial \mathbf{Q}_i^x}$:

$$\frac{\partial \mathbf{C}}{\partial \mathbf{Q}_i^x} = \sum_{j=1}^{3}\mathbf{Q}_j^x\mathbf{D}_i \otimes \mathbf{D}_j$$

If we note that $\mathbf{A} : (\mathbf{b}\otimes\mathbf{c}) = \mathbf{A}\mathbf{b}\cdot\mathbf{c}$ then we have :

$$\begin{aligned}
\frac{\partial W_P}{\partial \mathbf{Q}_i^x} &= \mathcal{A}_P\sum_{j=1}^{3}\mathbf{Q}_j^x(\mathbf{S}\mathbf{D}_i)\cdot\mathbf{D}_j = \mathcal{A}_P\sum_{j=1}^{3}((\mathbf{S}\mathbf{D}_i)\cdot\mathbf{D}_j)\mathbf{Q}_j^T \\
\mathbf{F}_i^{T_P} &= -\frac{\partial W_P}{\partial \mathbf{Q}_i}^T = -\mathcal{A}_P\sum_{j=1}^{3}((\mathbf{S}\mathbf{D}_i)\cdot\mathbf{D}_j)\mathbf{Q}_j \\
\mathbf{F}_i^{T_P} &= -\mathcal{A}_P\nabla\mathbf{\Phi}\ \mathbf{S}\ \mathbf{D}_i = -\mathcal{A}_P\ \mathbf{T}\ \mathbf{D}_i
\end{aligned}$$

Second, we show how the integration of the divergence of the first Piola-Kirchhoff stress tensor provides the same elastic force as in section III-E where we have simply taken the derivative of the energy with respect to the vertex position $\mathbf{Q}_i$. The same expression would have been obtained by applying the finite volume method over the dual barycentric grid as in [43]. Indeed, the Rayleigh-Ritz method, the finite element method and the finite volume method all produce the same nodal equations when a linear triangle element is used (constant strain).

From the differential equation 18, we build its *weak form* by invoking the principle of virtual work or the weighted residual method :

$$\int_\Omega(\nabla\cdot\mathbf{T} + \mathbf{R}(\mathbf{X}))wdA = \int_\Omega\rho\frac{\partial^2\mathbf{\Phi}(\mathbf{X})}{\partial t^2}wdA$$

where $w(\mathbf{X})$ is a test function that verifies the essential boundary conditions. In the remainder, we consider a vertex $\mathbf{P}$ and the set $S_\mathbf{P}$ of triangles adjacent to that point. We define a test function $w(\mathbf{X})$ as a hat function around $\mathbf{P}$, *i.e.* equal to 0 if $\mathbf{X}\notin S_\mathbf{P}$ and $w(\mathbf{X}) = \eta_i(\mathbf{X})$, if $\mathbf{X}\in T_P\subset S_\mathbf{P}$. If we only consider the elastic force, we can use the weak form to get the nodal elastic force at point $\mathbf{P}$:

$$\int_\Omega(\nabla\cdot\mathbf{T})wd\Omega = \sum_{T_P\in S_\mathbf{P}}\int_{T_P}(\nabla\cdot\mathbf{T})\eta_i(\mathbf{X})d\Omega = \sum_{T_P\in S_\mathbf{P}}\mathbf{F}_i^{T_P} = \mathbf{F}_i$$

We can further simplify the previous equation since the divergence satisfies : $div(\mathbf{T}w) = \mathbf{T}\nabla w + div(\mathbf{T})w$:

$$\sum_{T_P\in S_\mathbf{P}}\int_{T_P}div(\mathbf{T})\eta_i(\mathbf{X})d\Omega = \sum_{T_P\in S_\mathbf{P}}\int_{T_P}div(\mathbf{T}\eta_i) - (\mathbf{T}\,\nabla\eta_i)d\Omega$$

But since $\eta_i(\mathbf{X}) = 0$ if $\mathbf{X}\in\partial S_\mathbf{P}$ and according to Green's theorem the first term of the equation is null :

$$\int\int div(\mathbf{T}\eta_i)dA = \int_{\partial S_\mathbf{P}}(\mathbf{T}\eta_i)\cdot\mathbf{n}dl = 0$$

The gradient of the shape function $\nabla\eta_i$ being $\mathbf{D}_i$, we get a simple expression for the nodal force :

$$\begin{aligned}
\mathbf{F}_i &= \sum_{T_P\in S_\mathbf{P}}\int div(\mathbf{T})\eta_i(\mathbf{X})d\Omega \\
&= \sum_{T_P\in S_\mathbf{P}}\int -(\mathbf{T}\nabla\eta_i)d\Omega = \sum_{T_P\in S_\mathbf{P}} -\mathcal{A}_P\mathbf{T}\mathbf{D}_i
\end{aligned}$$

Acknowledgment

The author would like to thank the coauthors of SOFA platform and in particular Jérémie Allard, François Faure, Stéphane Cotin, Pierre-Jean Bensoussan, François Poyer, Christian Duriez and Laurent Grisoni.

References

[1] A. Nealen, M. Muller, R. Keiser, E. Boxerman, and M. Carlson, "Physically based deformable models in computer graphics." Eurographics State of the Art, Dublin, Ireland, Tech. Rep., Sept. 2005.

[2] M. Dauge, E. Faou, and Z. Yosibash, *Encyclopedia for Computational Mechanics*. Wiley, 2004, vol. I, ch. Plates and shells: Asymptotic expansions and hierarchical models.

[3] S. Green, "Multilevel, subdivision-based, thin shell finite elements: Development and an application to red blood cell modeling," Ph.D. dissertation, University of Washington, Feb. 2003.

[4] J. W. Eischen, S. Deng, and T. G. Clapp, "Finite-element modeling and control of flexible fabric parts," *IEEE Computer Graphics and Applications*, vol. 16, no. 5, pp. 71–80, Sept. 1996 1996, iSSN 0272-1716.

[5] F. Cirak, M. Ortiz, and P. Schröder, "Subdivision surfaces: new paradigm for thin-shell finite-element analysis," *International Journal for Numerical Methods in Engineering*, vol. 47, no. 12, p. 2039Ű2072, 2000.

[6] A. Van Gelder, "Approximate simulation of elastic membranes by triangulated spring meshes," *Journal of Graphics Tools: JGT*, vol. 3, no. 2, pp. 21–41, 1998.

[7] G. Bianchi, B. Solenthaler, G. Székely, and M. Harders, "Simultaneous topology and stiffness identification for mass-spring models based on fem reference deformations," in *Medical Image Computing and Computer-Assisted Intervention MICCAI 2004*, C. Barillot, Ed., vol. 2. Springer, November 2004, pp. 293–301.

[8] J. Louchet, X. Provot, and D. Crochemore, "Evolutionary identification of cloth animation models," in *Computer Animation and Simulation '95*, D. Terzopoulos and D. Thalmann, Eds., Eurographics. Springer-Verlag, Sept. 1995, pp. 44–54.

[9] D. Terzopoulos, J. Platt, A. Barr, and K. Fleischer, "Elastically deformable models," in *Computer Graphics (SIGGRAPH-87)*, vol. 21, no. 3, 1987, pp. 205–214.

[10] K. Waters and D. Terzopoulos, "Modeling and animating faces using scanned data," *The Journal of Visualization and Computer Animation*, vol. 2, pp. 129–131, 1991.

[11] A. Maciel, R. Boulic, and D. Thalmann, "Deformable tissue parameterized by properties of real biological tissue," in *International Symposium on Surgery Simulation and Soft Tissue Modeling (IS4TM'03)*, vol. 2673. Springer-Verlag Heidelberg, 2003, pp. 74–87.

[12] X. Provot, "Deformation constraints in a mass–spring model to describe rigid cloth behavior," in *Graphics Interface '95*, May 1995, pp. 147–154.

[13] D. E. Breen, D. H. House, and M. J. Wozny, "Predicting the drape of woven cloth using interacting particles," in *Proceedings of SIGGRAPH '94 (Orlando, Florida, July 24–29, 1994)*, ser. Computer Graphics Proceedings, Annual Conference Series, A. Glassner, Ed., ACM SIGGRAPH. ACM Press, July 1994, pp. 365–372.

[14] D. Baraff and A. Witkin, "Large steps in cloth simulation," in *Computer Graphics (SIGGRAPH'98)*, ACM, Ed., Orlando (USA), July 1998, pp. 43–54.

[15] J. Eischen and R. Bigliani, *Cloth Modeling and Animation*. A.K. Peters, 2000, ch. Continuum versus particle representations, pp. 19–122.

[16] D. Bourguignon and M.-P. Cani, "Controlling anisotropy in mass-spring systems," in *Computer Animation and Simulation '00*, ser. Eurographics, N. Magnenat-Thalmann, D. Thalmann, and B. Arnaldi, Eds. Springer-Verlag Wien New York, 2000, pp. 113–123, proceedings of the Eurographics Workshop in Interlaken, Switzerland, August 21–22, 2000.

[17] P. Volino, M. Courchesne, and N. M. Thalmann, "Versatile and efficient techniques for simulating cloth and other deformable objects," *Computer Graphics*, vol. 29, no. Annual Conference Series, pp. 137–144, Nov. 1995. [Online]. Available: http://www.acm.org:80/pubs/citations/proceedings/graph/218380/p137-volino/

[18] P. Volino and N. Magnenat-Thalmann, "Developing simulation techniques for an interactive clothing system," in *Proceedings of International Conference on Virtual Systems and MultiMedia*. Geneva, Switzerland: IEEE, 1997, pp. 109–118.

[19] O. Etzmuss, J. Gross, and W. Strasser, "Deriving a particle system from continuum mechanics for the animation of deformable objects," *IEEE Transactions on Visualization and Computer Graphics*, vol. 9, no. 4, pp. 538–550, Oct./Dec. 2003. [Online]. Available: http://csdl.computer.org/comp/trans/tg/2003/04/v0538abs.htm;http://csdl.computer.org/dl/trans/tg/2003/04/v0538.pdf

[20] E. Grinspun, A. N. Hirani, M. Desbrun, and P. Schröder, "Discrete shells," in *Eurographics/SIGGRAPH Symposium on Computer Animation*, D. Breen and M. Lin, Eds. San Diego, California: Eurographics Association, 2003, pp. 62–67. [Online]. Available: http://www.eg.org/EG/DL/WS/SCA03/062-067.pdf

[21] M. Teschner, B. Heidelberger, M. Mueller, and M. Gross, "A versatile and robust model for geometrically complex deformable solids," in *Computer Graphics International CGI'04*, Crete, Greece, 2004, pp. 312–319.

[22] O. Etzmuss, M. Keckeisen, and W. Straßer, "A Fast Finite Element Solution for Cloth Modelling," in *Proceedings of Pacific Graphics*, Canmore, Canada, 2003, pp. 244–252.

[23] B. Thomaszewski, M. Wacker, and W. Straßer, "A consistent bending model for cloth simulation with corotational subdivision finite elements," in *Proceedings of ACM SIGGRAPH/Eurographics Symposium on Computer Animation (SCA 2006)*. ACM Press, 2006, pp. 0–10.

[24] R. Bridson, S. Marino, and R. Fedkiw, "Simulation of clothing with folds and wrinkles," in *Eurographics/SIGGRAPH Symposium on Computer Animation*, D. Breen and M. Lin, Eds. San Diego, California: Eurographics Association, 2003, pp. 28–36. [Online]. Available: http://www.eg.org/EG/DL/WS/SCA03/028-036.pdf

[25] K.-J. Choi and H.-S. Ko, "Stable but responsive cloth," in *SIGGRAPH 2002 Conference Proceedings*, ser. Annual Conference Series, J. Hughes, Ed. ACM Press/ACM SIGGRAPH, 2002, pp. 604–611. [Online]. Available: http://visinfo.zib.de/EVlib/Show?EVL-2002-209

[26] P. Volino and N. Magnenat-Thalmann, "Simple linear bending stiffness in particle systems," in *Symposium on Computer Animation*. Eurographics/ACM.

[27] W. L. Briggs, V. E. Henson, and S. F. McCormick, *A Multigrid Tutorial*, second edition ed. The Society for Industrial and Applied Mathematics (SIAM), 2000.

[28] E. Grinspun, P. Krysl, and P. Schröder, "CHARMS: a simple framework for adaptive simulation," *ACM Transactions on Graphics*, vol. 21, no. 3, pp. 281–290, July 2002.

[29] S. Cotin, H. Delingette, and N. Ayache, "A hybrid elastic model allowing real-time cutting, deformations and force-feedback for surgery training and simulation," *The Visual Computer*, vol. 16, no. 8, pp. 437–452, 2000.

[30] X. Pennec, R. Stefanescu, V. Arsigny, P. Fillard, and N. Ayache, "Riemannian elasticity: A statistical regularization framework for non-linear registration," in *Proceedings of the 8th Int. Conf. on Medical Image Computing and Computer-Assisted Intervention - MICCAI 2005, Part II*, ser. LNCS, J. Duncan and G. Gerig, Eds., vol. 3750. Palm Springs, CA, USA, October 26-29: Springer Verlag, 2005, pp. 943–950.

[31] R. T. O. Zienkiewicz, *The Finite Element Method*, fifth ed. ed. Butterworth Heinemann, 2000, vol. Vol 1 : The Basis.

[32] P. Dluzewski, "Anisotropic hyperelasticity based upon general strain," *Journal of Elasticity*, vol. 60, no. 2, pp. 110–129, 2001.

[33] M. S. Floater and K. Hormann, *Advances in Multiresolution for Geometric Modelling*. Springer-Verlag, 2005, ch. Surface Parameterization: a Tutorial and Survey, pp. 157–186.

[34] G. Picinbono, H. Delingette, and N. Ayache, "Non-Linear Anisotropic Elasticity for Real-Time Surgery Simulation," *Graphical Models*, vol. 65, no. 5, pp. 305–321, Sept. 2003.

[35] M. Harders, "Surgical scene generation for virtual reality-based training in medicine," Thesis for the the venia legendi, SWISS FEDERAL INSTITUTE OF TECHNOLOGY ZURICH, Nov. 2006.

[36] V. Baudet, "Modélisation et simulation paramètrable d'objets déformables. application aux traitements des cancers pulmonaires." Ph.D. dissertation, Université Lyon I, June 2006.

[37] X. Wang and V. Devarajan, "1d and 2d structured mass-spring models with preload," *The Visual Computer*, vol. 21, no. 7, pp. 429–448, Aug. 2005.

[38] J. Teran, S. Blemker, V. N. T. Hing, and R. Fedkiw, "Finite volume methods for the simulation of skeletal muscle," in *Eurographics/SIGGRAPH Symposium on Computer Animation*, D. Breen and M. Lin, Eds. San Diego, California: Eurographics Association, 2003, pp. 68–74. [Online]. Available: http://www.eg.org/EG/DL/WS/SCA03/068-074.pdf

[39] G. Debunne, M. Desbrun, M.-P. Cani, and A. H. Barr, "Dynamic real-time deformations using space and time adaptive sampling," *Computer Graphics Proceedings*, Aug 2001, proceedings of SIGGRAPH'01.

[40] M. Nesme, F. Faure, and Y. Payan, "Hierarchical multi-resolution finite element model for soft body simulation," in *Workshop on Computer Assisted Diagnosis and Surgery*, Santiago de Chile, march 2006. [Online]. Available: http://www-evasion.imag.fr/Publications/2006/NFP06a

[41] K.-L. Bathe, *Finite Element Procedures in Engineering Analysis*. Prentice-Hall, 1982.

[42] M. Desbrun, M. Meyer, P. Schröder, and A. H. Barr, "Implicit fairing of irregular meshes using diffusion and curvature flow," *Computer Graphics*, vol. 33, no. Annual Conference Series, pp. 317–324, 1999. [Online]. Available: http://www.acm.org/pubs/citations/proceedings/graph/311535/p317-desbrun/

[43] J. Teran, E. Sifakis, S. S. Blemker, V. Ng-Thow-Hing, C. Lau, and R. Fedkiw, "Creating and simulating skeletal muscle from the visible human data set," *IEEE Transactions on Visualization and Computer Graphics*, vol. 11, no. 3, pp. 317–328, May/June 2005.